



جامعة الملك عبد الله  
للعلوم والتقنية

King Abdullah University of  
Science and Technology

## **Polarization Energies at Organic–Organic Interfaces: Impact on the Charge Separation Barrier at Donor–Acceptor Interfaces in Organic Solar Cells**

Item Type	Article
Authors	Ryno, Sean; Fu, Yao-Tsung; Risko, Chad; Bredas, Jean-Luc
Citation	Polarization Energies at Organic–Organic Interfaces: Impact on the Charge Separation Barrier at Donor–Acceptor Interfaces in Organic Solar Cells 2016 ACS Applied Materials & Interfaces
Eprint version	Post-print
DOI	<a href="https://doi.org/10.1021/acsami.6b02851">10.1021/acsami.6b02851</a>
Publisher	American Chemical Society (ACS)
Journal	ACS Applied Materials & Interfaces
Rights	This document is the Accepted Manuscript version of a Published Work that appeared in final form in ACS Applied Materials & Interfaces, copyright © American Chemical Society after peer review and technical editing by the publisher. To access the final edited and published work see <a href="http://pubs.acs.org/doi/abs/10.1021/acsami.6b02851">http://pubs.acs.org/doi/abs/10.1021/acsami.6b02851</a> .
Download date	09/08/2022 17:34:06
Link to Item	<a href="http://hdl.handle.net/10754/611771">http://hdl.handle.net/10754/611771</a>

## Article

**Polarization Energies at Organic–Organic Interfaces: Impact on the Charge Separation Barrier at Donor–Acceptor Interfaces in Organic Solar Cells**

Sean Ryno, Yao-Tsung Fu, Chad Risko, and Jean-Luc Bredas

*ACS Appl. Mater. Interfaces*, **Just Accepted Manuscript** • DOI: 10.1021/acsami.6b02851 • Publication Date (Web): 31 May 2016Downloaded from <http://pubs.acs.org> on June 5, 2016**Just Accepted**

“Just Accepted” manuscripts have been peer-reviewed and accepted for publication. They are posted online prior to technical editing, formatting for publication and author proofing. The American Chemical Society provides “Just Accepted” as a free service to the research community to expedite the dissemination of scientific material as soon as possible after acceptance. “Just Accepted” manuscripts appear in full in PDF format accompanied by an HTML abstract. “Just Accepted” manuscripts have been fully peer reviewed, but should not be considered the official version of record. They are accessible to all readers and citable by the Digital Object Identifier (DOI®). “Just Accepted” is an optional service offered to authors. Therefore, the “Just Accepted” Web site may not include all articles that will be published in the journal. After a manuscript is technically edited and formatted, it will be removed from the “Just Accepted” Web site and published as an ASAP article. Note that technical editing may introduce minor changes to the manuscript text and/or graphics which could affect content, and all legal disclaimers and ethical guidelines that apply to the journal pertain. ACS cannot be held responsible for errors or consequences arising from the use of information contained in these “Just Accepted” manuscripts.

1  
2  
3  
4  
5  
6  
7 **Polarization Energies at Organic–Organic Interfaces:**  
8  
9  
10 **Impact on the Charge Separation Barrier at Donor–Acceptor**  
11  
12  
13 **Interfaces in Organic Solar Cells**  
14  
15  
16  
17  
18  
19  
20

21 **Sean M. Ryno,<sup>‡,¶</sup> Yao-Tsung Fu,<sup>¶</sup> Chad Risko,<sup>#,\*</sup> and Jean-Luc Brédas<sup>‡,\*</sup>**  
22  
23

24 *<sup>‡</sup>Solar and Photovoltaics Engineering Research Center*  
25 *King Abdullah University of Science and Technology*  
26 *Thuwal 23599-6900, Kingdom of Saudi Arabia*  
27

28  
29 *<sup>¶</sup>School of Chemistry and Biochemistry &*  
30 *Center for Organic Photonics and Electronics*  
31 *Georgia Institute of Technology*  
32 *Atlanta, Georgia 30332-0400*  
33

34  
35 *<sup>#</sup>Department of Chemistry &*  
36 *Center for Applied Energy Research*  
37 *University of Kentucky*  
38 *Lexington, Kentucky 40506-0055*  
39  
40  
41  
42  
43  
44  
45  
46  
47  
48  
49  
50  
51  
52

53  
54 \*Corresponding authors: chad.risko@kyu.edu; jean-luc.bredas@kaust.edu.sa  
55  
56  
57  
58  
59  
60

## Abstract

We probe the energetic landscape at a model pentacene/fullerene-C<sub>60</sub> interface to investigate the interactions between positive and negative charges, which are critical to the processes of charge separation and recombination in organic solar cells. Using a polarizable force field, we find that polarization energy, *i.e.* the stabilization a charge feels due to its environment, is larger at the interface than in the bulk for both a positive and a negative charge. The combination of the charge being more stabilized at the interface and the Coulomb attraction between the charges, results in a barrier to charge separation at the pentacene-C<sub>60</sub> interface that can be in excess of 0.7 eV for *static* configurations of the donor and acceptor locations. However, the impact of molecular motions, *i.e.*, the dynamics, at the interface at room temperature results in a distribution of polarization energies and in charge separation barriers that can be significantly reduced. The dynamic nature of the interface is thus critical, with the polarization energy distributions indicating that sites along the interface shift in time between favorable and unfavorable configurations for charge separation.

**Keywords:** organic photovoltaics, charge separation and recombination, polarization, organic-organic interfaces, molecular dynamics, multiscale modelling, energetic disorder

## Introduction

Organic photovoltaics (OPV) hold promise of providing large-area, low-cost solar energy conversion, with current multijunction devices exceeding 13% power conversion efficiency,<sup>1-2</sup> and single-layer devices now approaching 12%.<sup>3-5</sup> The active layers of these devices typically consist of two components, an electron donor and an electron acceptor, in either a bilayer structure or as a blend termed a bulk heterojunction. Morphology plays a critical role in the efficiencies of the various electronic and optical processes involved in solar-cell operation, including optical absorption, exciton formation, exciton migration, exciton dissociation, charge recombination, charge transport, and charge collection.<sup>6</sup> While the importance of the donor-acceptor interface has been acknowledged in previous investigations,<sup>7-15</sup> of particular focus over the past few years has been the purity of the interface between the two materials. What was once thought to be fairly clear-cut interfaces between the donor and acceptor components, has been replaced by a complex morphological picture that includes pure domains with different extents of ordered and disordered packing as well as intermixed regions of the two materials where charge generation primarily occurs.<sup>16-28</sup>

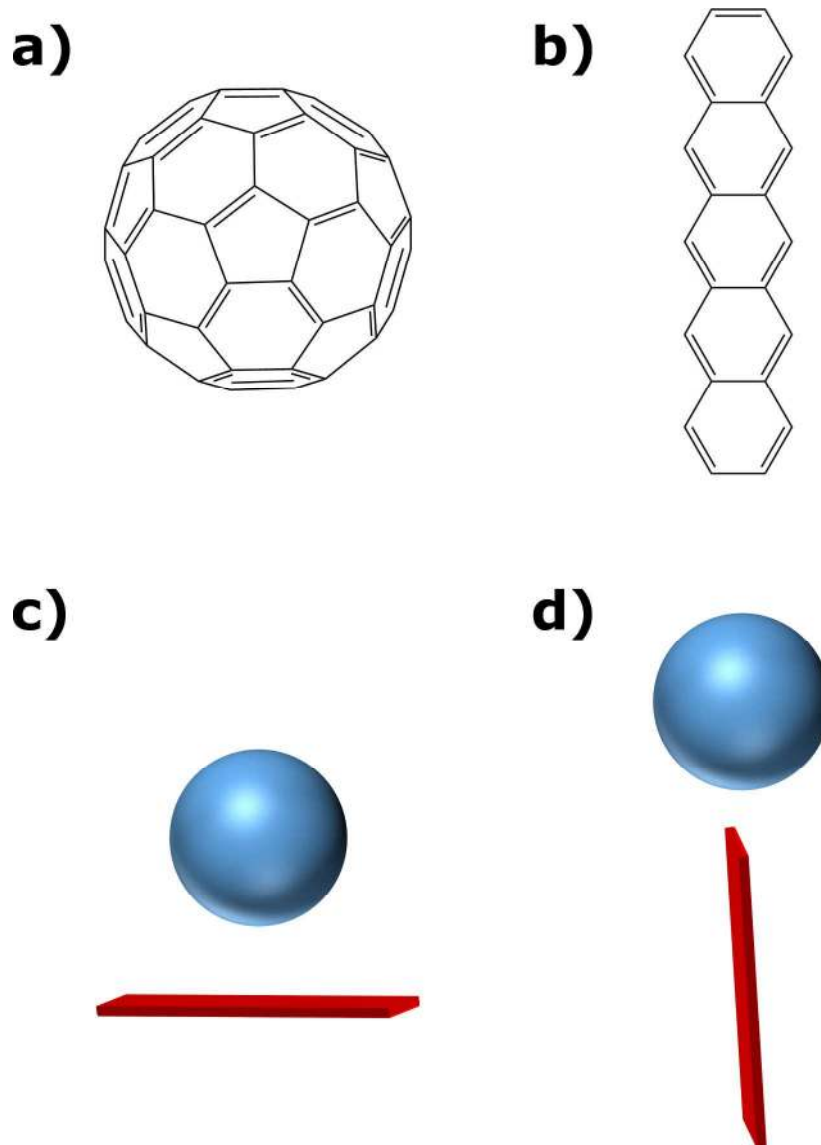
As we discussed recently,<sup>29</sup> the energetic landscape at a surface (*i.e.*, organic-vacuum interface) differs significantly from the bulk of a crystalline material. One would expect, furthermore, the addition of a second organic component to further complicate the landscape. In the bulk of an organic molecular crystal or at an organic-vacuum interface, all molecular sites are essentially identical, except for the difference in site energies due to nonequivalent molecules and dynamic fluctuations. In contrast, at organic-organic interfaces, the molecular sites reside in distinct environments, which will result in a distribution of site energies or polarization energies. Because of the anisotropic nature of the environment, the barrier to charge separation is expected

1  
2  
3 to vary from molecular site to molecular site. Here, in order to better understand the environment  
4 of charge carriers at the donor-acceptor interface and to determine the impact of molecular  
5 motions on the charge separation process, we use a combination of molecular dynamics (MD)  
6 simulations together with the methodology we developed<sup>21,30-31</sup> for determining electronic  
7 polarization energy in organic molecular crystals. Our goal is to gain a picture of the energetic  
8 landscape at a disordered donor-acceptor interface and to investigate the landscape dynamics,  
9 *i.e.*, how it changes with time.  
10  
11  
12  
13  
14  
15  
16  
17  
18  
19

20  
21 We take the pentacene/C<sub>60</sub> interface as a representative model, see Figure 1. It is useful to recall  
22 that Verlaak *et al.* showed previously, using a static (*i.e.*, fixed) configuration of the interface,  
23 that an ideal *edge-on* pentacene (001)/C<sub>60</sub> interface presents a barrier of approximately 0.4 eV to  
24 charge separation, while charge separation at a *face-on* pentacene (01-1)/C<sub>60</sub> interface is quasi-  
25 barrierless, leading one to assume that the *face-on* orientation is preferable.<sup>12</sup> Yi *et al.*<sup>11</sup>,  
26 however, underlined that this is not necessarily the case, as the rate of charge recombination is  
27 calculated to be several orders-of-magnitude faster for the *face-on* orientation than the *edge-on*  
28 orientation.  
29  
30  
31  
32  
33  
34  
35  
36  
37  
38  
39

40  
41 This work is structured as follows. We begin by determining the polarization energy of a positive  
42 charge carrier in bulk pentacene and a negative charge carrier in bulk C<sub>60</sub> and obtain good  
43 agreement with experiment. To assess the impact of molecular orientation at an interface, we  
44 then consider model interfaces where pentacene is either *face-on* or *edge-on*. Finally, we  
45 examine a bilayer interface composed of bulk pentacene and C<sub>60</sub> to assess the polarization energy  
46 at molecular sites along the interface and into the bulk; we do so not only for static but also  
47 dynamic frameworks to determine how the polarization energy varies as a function of time. At  
48 sites along the interface, we evaluate the geminate pair energies, *i.e.*, when the charges are  
49  
50  
51  
52  
53  
54  
55  
56  
57  
58  
59  
60

1  
2  
3 allowed to interact, and the non-interacting electron-hole energies, *i.e.*, the change in the energy  
4 of the system due to the presence of the hole and electron when they are unable to see each other,  
5  
6 to examine the fluctuations with time of the barrier to charge separation.  
7  
8  
9  
10  
11  
12  
13  
14



55  
56  
57  
58  
59  
60

**Figure 1.** Chemical structures of the C<sub>60</sub> fullerene (a) and pentacene (b). Graphical representations of the (c) *face-on* pentacene/C<sub>60</sub> and (d) *edge-on* pentacene/C<sub>60</sub> complexes.

## Methodology

All polarization energies were calculated via the AMOEBA force field of Ren and Ponder.<sup>32-33</sup>

The geometries of isolated pentacene molecules used for the AMOEBA force field parameterization, one-dimensional, stacked interfaces, and the unit cells that were replicated and from which spherical bulk clusters and slabs were extracted, for bulk and interfacial systems, respectively, were obtained from the Cambridge Structural Database (PENCEN04).<sup>34-35</sup> The Materials Studio 6.1 software suite was used to create a face-centered cubic C<sub>60</sub> packing configuration where  $\alpha = \beta = \gamma = 60^\circ$  and  $a = b = c = 9.943 \text{ \AA}$  for the reduced cell and  $\alpha = \beta = \gamma = 90^\circ$  and  $a = b = c = 14.062 \text{ \AA}$  for the conventional cell, mirroring the unit cell parameters reported by Ibers and co-workers (SOCTOT23) without the positional disorder present in the reported crystal structure.<sup>36</sup>

To generate force field parameters, atom-centered multipoles were obtained with Stone's GDMA program via distributed multipole analysis of the single-particle density matrices.<sup>37</sup> To derive the density matrices, single-point energy calculations at the MP2/6-31+G(d,p) and DFT/B97D/6-31+G(d,p) level were performed on neutral, positively charged, and negatively charged pentacene, while single-point energy calculations at the DFT/B97D/6-31+G(d,p) level were completed for neutral and negatively charged C<sub>60</sub> using the Gaussian 09 software suite.<sup>38</sup> Additional information on force-field parameterization is available in Ref. 29.

As a first step to exploring the effects of an organic-organic interface on the polarization energy due to an excess charge carrier, we determined the polarization energies of the respective bulk



1  
2  
3 materials. In our previous investigations of electronic polarization energy, the parameterization  
4 of the electrostatic component of the AMOEBA force field was carried out via *ab initio* MP2  
5 calculations followed by a distributed multipole analysis (DMA) to generate atom-centered  
6 multipoles.<sup>30-31</sup> As shown in Figure S1, this parameterization procedure leads to the excess  
7 charge in the anion becoming localized to one portion of the C<sub>60</sub> molecule. To obtain a charge  
8 distribution in which the charge is delocalized across the entirety of C<sub>60</sub>, as one would expect  
9 from previous theoretical studies,<sup>39-40</sup> the parameterization of the electrostatic component was  
10 carried out using density functional theory at the B97D level.<sup>41</sup> This method results in the  
11 negative charge of the C<sub>60</sub> radical anion being evenly distributed across the entire molecule; the  
12 charge distributions for the radical-anion and radical-cation states of pentacene, as in the MP2  
13 calculations, are distributed symmetrically across the entire molecule. Additional details of the  
14 validation of this new parameterization procedure are available in the Supporting Information.  
15  
16  
17  
18  
19  
20  
21  
22  
23  
24  
25  
26  
27  
28  
29  
30  
31

32 Considering a given cluster of molecules, the polarization energy is calculated using the Lyons  
33 model.<sup>42</sup>  
34  
35  
36  
37

$$P_+ = IE_{ss} - IE_g$$

38  
39  
40  
41  
42 where  $P_+$  is the polarization energy due to a positive charge and  $IE$  is the solid-state or gas-  
43 phase ionization energy, respectively; there exists an analogous equation for the polarization due  
44 to a negative charge,  $P_-$ , involving the electron affinities. The bulk polarization energy is  
45 determined by increasing the radius of spherical clusters and plotting the calculated polarization  
46 energies versus  $1/N^3$ , where  $N$  is the number of molecules in the cluster, and extrapolating to  
47 infinite system size.<sup>30,42-43</sup>  
48  
49  
50  
51  
52  
53  
54  
55  
56  
57  
58  
59  
60

Model one-dimensional (1D) interfaces were constructed using the isolated geometries from above, wherein each pentacene or C<sub>60</sub> was replicated along one dimension to give a stacked interface in either a *face-on* or *edge-on* configuration (Figure 2). While both of these configurations differ significantly from what is observed for the actual materials (*i.e.*, within layers pentacene packs in a herringbone fashion and molecules do not sit perfectly on top of one another), these simplified interfaces allow for the limit of perfect order to be probed without introducing the complexity of molecular rotation. Molecules within the 1D interfaces are separated by 3.5 Å with a 3.5 Å separation at the pentacene/C<sub>60</sub> interface. Additionally, possible band bending at the interface is evaluated by placing either a positive or negative charge at the interface and moving it towards the bulk.

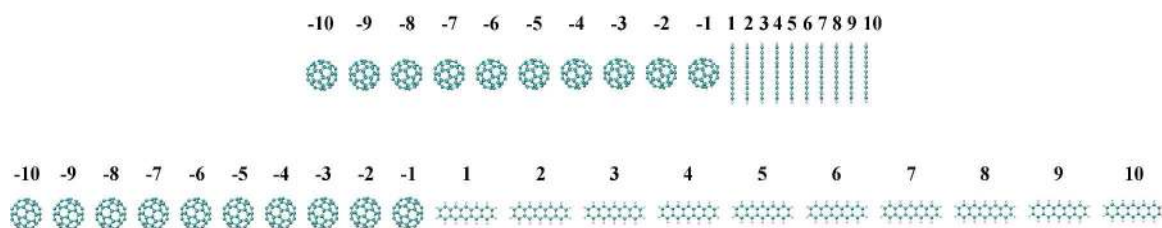


**Figure 2.** (Top) *Face-on* pentacene/C<sub>60</sub> and (bottom) *edge-on* pentacene/C<sub>60</sub> one-dimensional interfaces together with the numbering of the molecular sites. Note that only the six closest molecules to the interface have been considered for the polarization energy and induced-dipole calculations as additional molecules introduce artifacts from the organic-vacuum interface at the edges of the systems.

Model pentacene(001)/C<sub>60</sub>(001) three-dimensional (3D) interfaces were created by placing a C<sub>60</sub>(001) slab (6.8 nm x 6.8 nm x 14 layers) on top of a pentacene (001) slab (6.8 nm x 6.8 nm x 8.6 nm) together with a large vacuum space along the *z* direction to limit supercell periodicity to

1  
2  
3 the  $xy$ -plane, resulting in a cell of ( $x=$ ) 6.8 nm x ( $y=$ ) 6.8 nm x ( $z=$ ) 50 nm. This was followed by  
4  
5 a molecular mechanics MM3<sup>44</sup> minimization to optimize the separation distance at the interface.  
6  
7 Following the methodology of Fu *et al.*,<sup>21</sup> we used this configuration as the initial configuration  
8  
9 for molecular dynamics (MD) simulations in the NVT ensemble at 300 K with the velocity  
10  
11 Verlet integrator<sup>45</sup> and Berendsen thermostat.<sup>46</sup> A spherical cutoff of 12 Å was implemented for  
12  
13 the summation of van der Waals interactions and Ewald summation<sup>47</sup> for Coulomb interactions.  
14  
15 The rattle algorithm<sup>48</sup> was employed to constrain C-H bonds. This system was equilibrated for 1  
16  
17 ns and then replicated in each of the  $x$  and  $y$  directions to give a final supercell of 13.7 nm x 13.7  
18  
19 nm x 50 nm composed of 4752 pentacene and 2744 C<sub>60</sub> molecules. The supercell was then  
20  
21 allowed to further evolve over 10 ps for final equilibration and over another 10 ps for data  
22  
23 collection. The largest energy fluctuation during data collection was about 0.02% of the total  
24  
25 energy with a standard deviation of less than 0.01%. Polarization energies at various sites at the  
26  
27 interface and sites in layers moving away from the bulk were then calculated. All MD  
28  
29 simulations were carried out using the Tinker code.<sup>49</sup>  
30  
31  
32  
33  
34  
35  
36  
37  
38  
39  
40

## 41 **Results and Discussion**

### 42 ***Bulk Polarization Energy***

43  
44 Since pentacene acts as an electron-donor and C<sub>60</sub> acts as an electron-acceptor in the systems we  
45  
46 wish to investigate, we first determine the bulk polarization energy due to a positive charge in  
47  
48 pentacene and a negative charge in C<sub>60</sub> via our revised parameterization procedure. While there  
49  
50 have been a number of studies to determine the polarization energy due to a positive charge in  
51  
52 pentacene,<sup>35,50-53</sup> evaluations of the polarization energy in C<sub>60</sub> due to a positive or negative  
53  
54  
55  
56  
57  
58  
59  
60

charge have been limited to the investigations of Sato and co-workers<sup>54</sup> and of Yoshida,<sup>55</sup> who evaluated the polarization energy in a series of fullerenes. Using the gas-phase and solid-state ionization energies determined by Lichtenberger and co-workers,<sup>56</sup>  $P_{+,C_{60}}$  is 1.1 – 1.4 eV; by comparison to available gas-phase electron affinity (EA) data,  $P_{-,C_{60}}$  is in the range 1.4 – 1.6 eV, that is, it is either equal to, or greater by up to 0.5 eV than  $P_{+,C_{60}}$ . These numbers suggest that  $P_- \geq P_+$  in  $C_{60}$ , which is opposite to the trend observed for the unsubstituted linear oligoacenes, *i.e.*,  $P_- < P_+$ .<sup>30</sup> This results from the absence of a molecular quadrupole in  $C_{60}$  and, thus, no contribution from charge-permanent quadrupole interactions. As a consequence, the polarization energy is determined mainly by induced-dipole interactions, though it is important to point out that there occur higher-order charge-permanent multipole interactions. If one assumes an equal but oppositely signed charge distribution for the  $C_{60}$  anion and cation, then it is expected that  $P_- = P_+$ , which is one of the limits found experimentally (we note that if the charge distributions are not equivalent and such that the cation is delocalizing more than the anion, a situation where  $P_- > P_+$  would result due to larger induced dipoles near the regions with larger charge density). Indeed, we find that the charge distributions for the hole and electron are similar and opposite in sign. This results in a calculated polarization energy due to a negative charge carrier in  $C_{60}$  to be nearly equivalent to the polarization due to a positive charge carrier, 0.72 eV and 0.75 eV, respectively.

Experimentally, if we take for the polarization energy due to a negative charge carrier on a  $C_{60}$  molecule ( $P_{-,C_{60}}$ ) the value of 1.4 eV at which  $P_{+,C_{60}} = P_{-,C_{60}}$ ,<sup>51,54</sup> there is an estimated difference of about 0.2 eV with the polarization energy due to a positive charge carrier in pentacene ( $P_{+,P5}$ ),

1  
2  
3  
4  
5  
6  
7  
8  
9  
10  
11  
12  
13  
14  
15  
16  
17  
18  
19  
20  
21  
22  
23  
24  
25  
26  
27  
28  
29  
30  
31  
32  
33  
34  
35  
36  
37  
38  
39  
40  
41  
42  
43  
44  
45  
46  
47  
48  
49  
50  
51  
52  
53  
54  
55  
56  
57  
58  
59  
60

1.6 eV. Using our model, we calculated each of the respective bulk polarization energies through extrapolation of the polarization energy of finite clusters. We find that the polarization energy of a positive charge carrier in pentacene (0.99 eV) is calculated to be some 0.27 eV larger than that of a negative charge carrier in  $C_{60}$  (0.72 eV), see Figure 3. This is in general agreement with the calculations of D'Avino *et al.* who applied both microelectrostatic and semiempirical models to the bulk of pentacene and  $C_{60}$  and obtained differences,  $P_{+,P5} - P_{-,C60}$ , of 0.07 eV and 0.16 eV, respectively,<sup>14</sup> and the work of Gorczak *et al.*<sup>13</sup> who determined a difference of 0.31 eV.

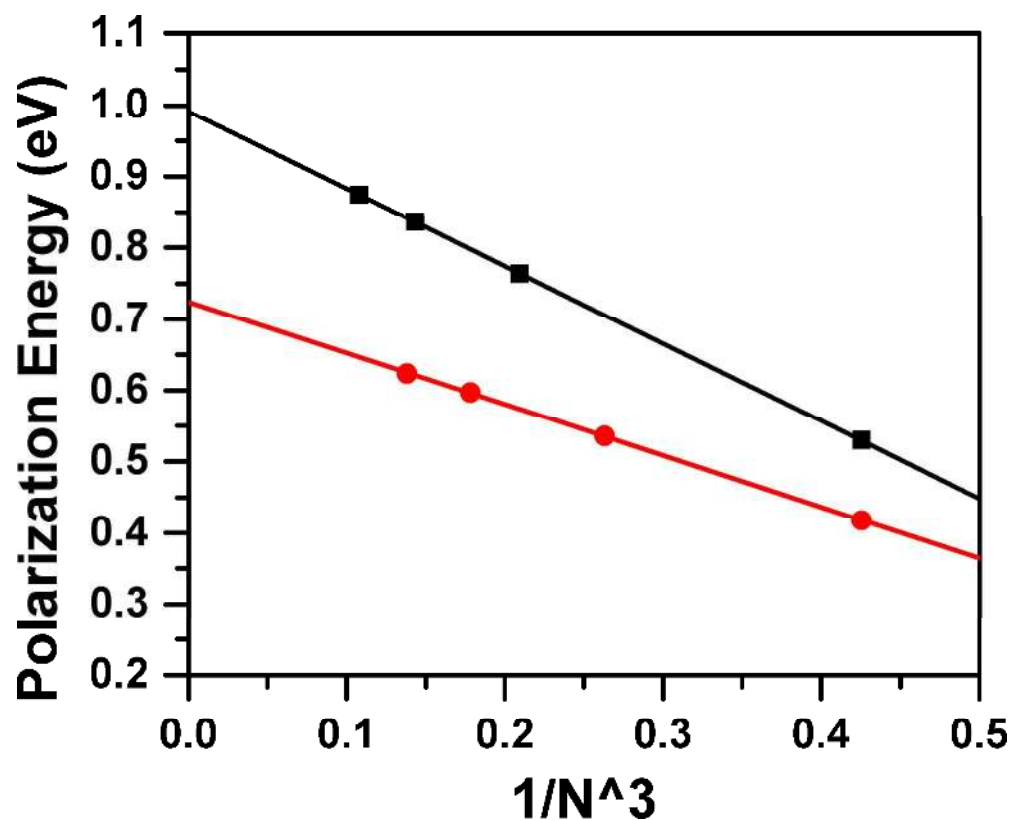


**Figure 3.** Electronic polarization energies for a positive charge in pentacene (black) and negative charge in  $C_{60}$  (red).

### Band Bending in One-Dimensional Stacks

To compare with previous theoretical results and provide an additional step of validation,<sup>9-10</sup> we evaluated the band bending in the one-dimensional donor-acceptor chains illustrated in Figure 2. These 1D chains also allow us to use a step-up approach and examine how the interactions change as the complexity of the system increases. Within 1D model interfaces, we chose to have each molecule separated by 3.5 Å, so as to be consistent with the work of Idé *et al.*<sup>57</sup> We begin with a neutral system and then place a charge on either pentacene (site 1) or C<sub>60</sub> (site -1) at the interface and move the charge to the nearest-neighbor away from the interface. At each site, the IE or EA is calculated as a function of molecular position (Figure 4). The same plot as a function of distance rather than site is available in the SI (Figure S2).

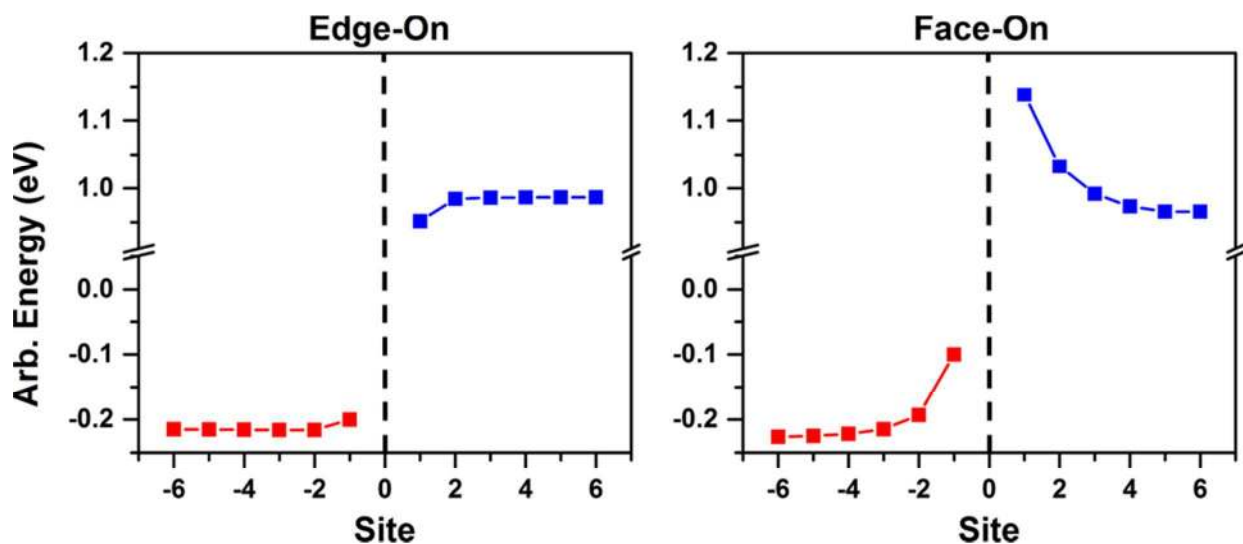


**Figure 4.** Shift in the ionization energy of pentacene (blue) and electron affinity of C<sub>60</sub> (red) for an *edge-on* pentacene/C<sub>60</sub> interface (left) and *face-on* pentacene/C<sub>60</sub> interface (right). A more negative value for the EA represents a larger, *i.e.*, more stabilizing, EA. For the IE, a more positive value represents a larger IE, *i.e.*, less stabilizing.

1  
2  
3 There is a destabilization of the electron on C<sub>60</sub> as it is moved towards the interface for both  
4 orientations of pentacene, with the *face-on* pentacene configuration presenting a larger  
5 destabilization. This is a result of the larger interactions between a charge on C<sub>60</sub> and the  
6 quadrupole on pentacene in the *face-on* orientation and the increased magnitude of the induced  
7 dipoles, as previously reported by Linares *et al.*<sup>9</sup> Also note, as we have recently shown,<sup>29</sup> that for  
8 the model chain of *edge-on* pentacenes, which is similar to the *interlayer* packing in bulk  
9 pentacene (packing along the *c*-axis), the band bending and thus the polarization energy changes  
10 very little after moving one layer from the interface (*i.e.*, sites other than 1 or 2). For the *face-on*  
11 orientation, which is somewhat similar to the *intralayer* packing (*ab*-plane), the band bending  
12 falls off much more slowly, not saturating until the charge is on site-5 for pentacene; this is  
13 consistent with the behavior observed in the bulk, where the polarization energy does not  
14 stabilize until about 4 nm (~10 molecular sites in pentacene) from the charge carrier.<sup>30</sup> For  
15 pentacene, there is also a qualitative change in the band bending since a hole is destabilized at  
16 the interface for a *face-on* pentacene interface and stabilized at the *edge-on* interface. Again, this  
17 results from the change in charge-quadrupole interactions; in the *edge-on* orientation, the  
18 positively charged pentacene interacts with small positive quadrupoles on the neighboring  
19 pentacene while in the *face-on* orientation the charged pentacene interacts with a large negative  
20 quadrupole.<sup>57</sup> Thus, as the charge moves away from the interface in the *edge-on* system, there are  
21 additional destabilizing like-signed charge-quadrupole interactions, while in the *face-on*  
22 interfaces there are additional stabilizing opposite-signed charge-quadrupole interactions.

23  
24  
25 Looking more closely at the neutral systems, there is an induced dipole at the interface due to the  
26 quadrupole moment of pentacene, as discussed by Idé *et al.*<sup>57</sup> This induced dipole impacts not  
27 only the molecules at the interface but also induces dipole moments along the chain although

1  
2  
3 with lessening strength as one moves away from the interface. Depending on the orientation of  
4  
5 the pentacenes, the direction of the induced dipole is different as the sign of the quadrupole  
6  
7 component closest to  $C_{60}$  changes, *i.e.*, the induced dipole points towards the  $C_{60}$  bulk for *face-on*  
8  
9 pentacene and towards the pentacene bulk for *edge-on* pentacene (Figure 5). Also note that the  
10  
11 induced dipole is an order-of-magnitude smaller for the *edge-on* pentacene configuration, a result  
12  
13 of the small quadrupole moment and larger distance between additional atom-centers.  
14  
15  
16

17  
18 Thus, in the case of model, highly ordered one-dimensional chains, it is found that the driving  
19  
20 force for charges to move away from the interface is small for the *edge-on* pentacene orientation  
21  
22 and quite large for the *face-on* orientation. These differences stem from a combination of  
23  
24 permanent multipole and induced-dipole contributions. If the orientation of just a few molecules  
25  
26 presents such pronounced effects on a charge at the interface, then the effects of many additional  
27  
28 neighbors, resulting in variations in the electrostatic environment of each molecule, should be  
29  
30 expected to have an important impact.  
31  
32  
33  
34  
35  
36  
37  
38

### 39 ***Polarization Energy and Induced Dipoles in Model Bilayer Interfaces***

40  
41  
42 We now consider the polarization energies due to the presence of either a single positive or  
43  
44 negative at an idealized *edge-on* pentacene/ $C_{60}$  interface, created by layering crystalline surfaces  
45  
46 of pentacene and  $C_{60}$ , followed by minimization using the MM3 force field to optimize the  
47  
48 *intermolecular* separation distances at the interface, see Figure S3. Even when examining such a  
49  
50 static model interface,<sup>9,12-13</sup> it is readily seen in Figure 6 that there is a broad range of  
51  
52 polarization energies within the interfacial layers of pentacene and  $C_{60}$ , making each site  
53  
54 distinctive. For pentacene, the polarization energy due to a positive charge carrier in a 4-nm  
55  
56  
57  
58  
59  
60



1  
2  
3 radius cluster, ranges from 0.76 eV to 0.92 eV, while a negative charge carrier in C<sub>60</sub> has a  
4  
5 polarization stabilization between 0.56 eV and 0.81 eV.<sup>58</sup> The 0.2 to 0.3 eV range in polarization  
6  
7 energy between sites suggests that the electrostatic environment of each molecule varies  
8  
9 significantly due to the presence and packing configurations of the additional organic material.  
10  
11  
12  
13  
14  
15  
16  
17  
18  
19  
20  
21  
22  
23  
24  
25  
26  
27  
28  
29  
30  
31  
32  
33  
34  
35  
36  
37  
38  
39  
40  
41  
42  
43  
44  
45  
46  
47  
48  
49  
50  
51  
52  
53  
54  
55  
56  
57  
58  
59  
60

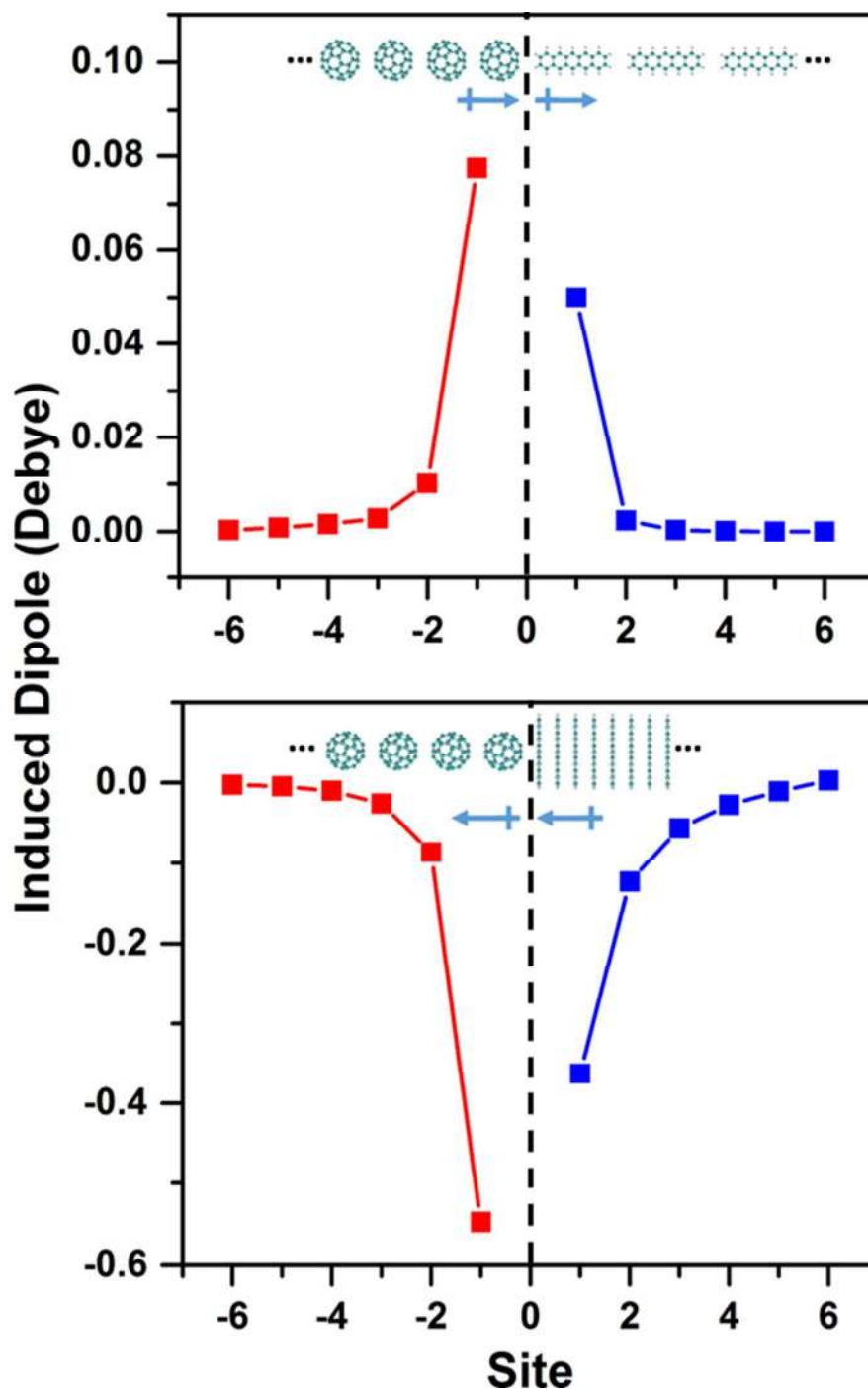


**Figure 5.** Induced dipoles on pentacene (blue) and C<sub>60</sub> (red) at a model one-dimensional interface in the absence of any net charge, where each molecular site is separated by 3.5 Å in an *edge-on* orientation (top) and a *face-on* orientation (bottom). Insert: Illustration of the orientation of the induced dipoles of the interfacial molecules and representation of the molecular systems.

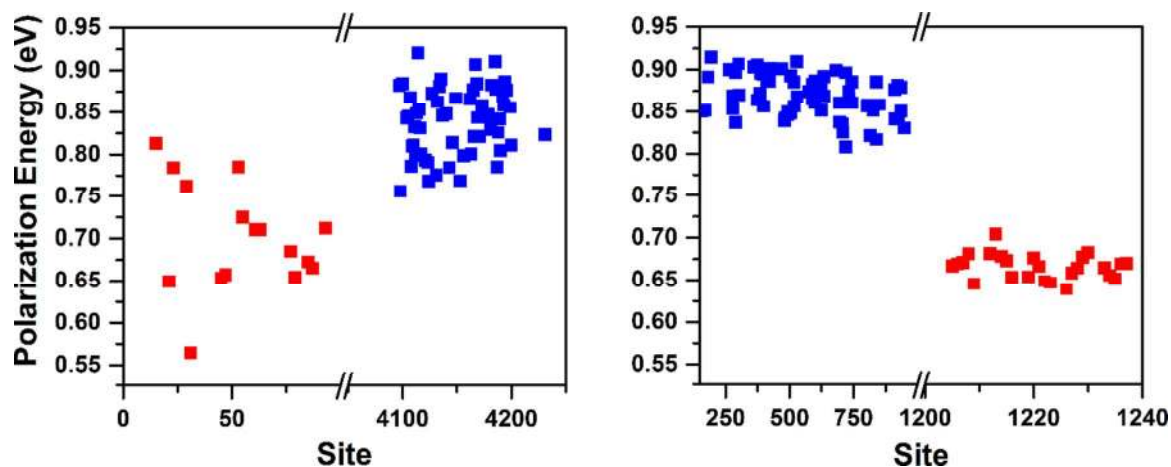


**Figure 6.** Polarization energy for a negative charge carrier in C<sub>60</sub> (red) and a positive charge carrier in pentacene (blue) in the interfacial layers of the two organic components within spherical clusters with a 4-nm radius. Two systems are considered: (Left) A slab of pentacene and a slab of C<sub>60</sub> glued together followed by a MM3 minimization. (Right) The same system after 1 ns of molecular dynamics simulation at 300 K.

The MD simulations of Fu *et al.* showed that the pentacene(001)/C<sub>60</sub> interface (*i.e.*, a *face-on* type interface) is more complex than is typically accounted for, with the pentacene molecules migrating from the interfacial layer to the divots between the neighboring C<sub>60</sub> molecules, resulting in a mixed, disordered interface.<sup>21</sup> To provide a more complete picture than the static interface composed of two slabs brought to close contact, the MM3 force field was used for MD simulations to model a disordered interface due to the dynamic processes that occur at room temperature. The C<sub>60</sub> molecules are found to take on a hexagonal closed packing configuration as reported previously.<sup>21</sup>

We considered 25 C<sub>60</sub> and 71 pentacene molecules at the interface, extracted from a single MD snapshot after equilibration was reached, for comparison to the molecular-mechanics minimized static interface and analysis of how the interface changes after 1 ns of simulation at 300 K. Note that the molecular sites are not identical, as highlighted by the large variation in the induced

1  
2  
3 dipole for sites along the interface (Figure 7). Note, also, that there does not appear to be a  
4 correlation between the sign and magnitude of the induced dipole of a specific site and other sites  
5 that are similar via visual inspection. The largest qualitative difference between the minimized  
6 slab interface and the interface after being treated by MD is the narrowing of the distribution of  
7 site polarization energies at the interface and an increase in the average difference between the  
8 polarization energies due to a positive or negative charge (0.14 eV, minimized; 0.21 eV,  
9 dynamic); the average polarization energy due to each charge type also increases by 0.1 eV. This  
10 indicates that during the MD simulations the thermal fluctuations act to minimize the overall  
11 differences among molecular sites, while still keeping them distinct. It is interesting to note that  
12 while the site polarization energies are more uniform in the MD snapshot, the sites display a  
13 large number of configurations, including pentacene partially moving from the pentacene layer  
14 to the space between C<sub>60</sub> molecules. These types of dislocations do not result in large changes in  
15 polarization energy, but do impact charge separation as discussed later.  
16  
17  
18  
19  
20  
21  
22  
23  
24  
25  
26  
27  
28  
29  
30  
31  
32  
33  
34

35 Using this same snapshot, we probe molecular sites as the charge is moved away from the  
36 interface towards the bulk to see how the polarization energy changes as a function of molecular  
37 layer, see Figure 8. First focusing on pentacene, we observe that there is a large change in the  
38 polarization energy when moving from the interfacial layer of pentacene to one layer from the  
39 interface and then little change upon moving farther from the interface. In contrast to an organic-  
40 vacuum interface, where the polarization energy at the interface is lower than the bulk (0.07 eV  
41 in tetracene),<sup>29</sup> the average polarization energy (1.00 eV, pentacene; 0.80 eV, C<sub>60</sub>) at the  
42 considered organic-organic interface is larger than in the bulk (0.95 eV, pentacene; 0.76 eV,  
43 C<sub>60</sub>). At the organic-vacuum interface, there is a reduction in the amount of stabilizing  
44 polarizable material and destabilizing permanent quadrupoles resulting in a net smaller  
45  
46  
47  
48  
49  
50  
51  
52  
53  
54  
55  
56  
57  
58  
59  
60

1  
2  
3 polarization energy,<sup>29</sup> while at the pentacene/C<sub>60</sub> interface, a polarizable material (*i.e.*, C<sub>60</sub>) is still  
4  
5 present, but the destabilizing permanent quadrupoles that would have otherwise been present due  
6  
7 to pentacene have been removed. Thus, there is a net increase in the polarization energy of sites  
8  
9 along the pentacene/C<sub>60</sub> interface.  
10  
11  
12  
13  
14  
15  
16  
17  
18  
19

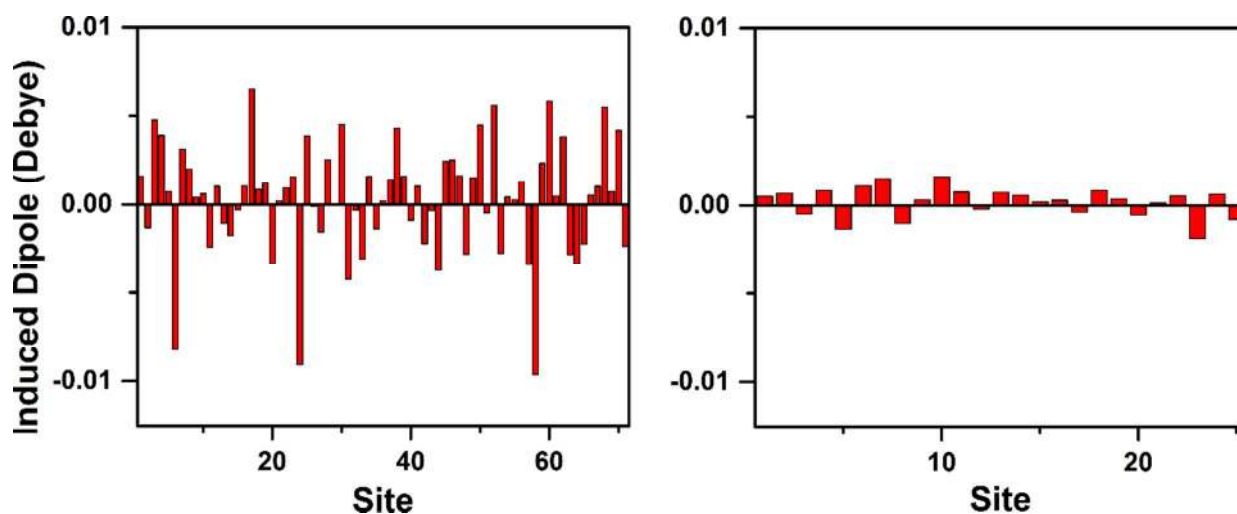


**Figure 7.** The *z*-component of the induced dipole on pentacene (left) and C<sub>60</sub> (right), as a function of molecular site at a neutral *edge-on* interface. Site numbers are arbitrary.

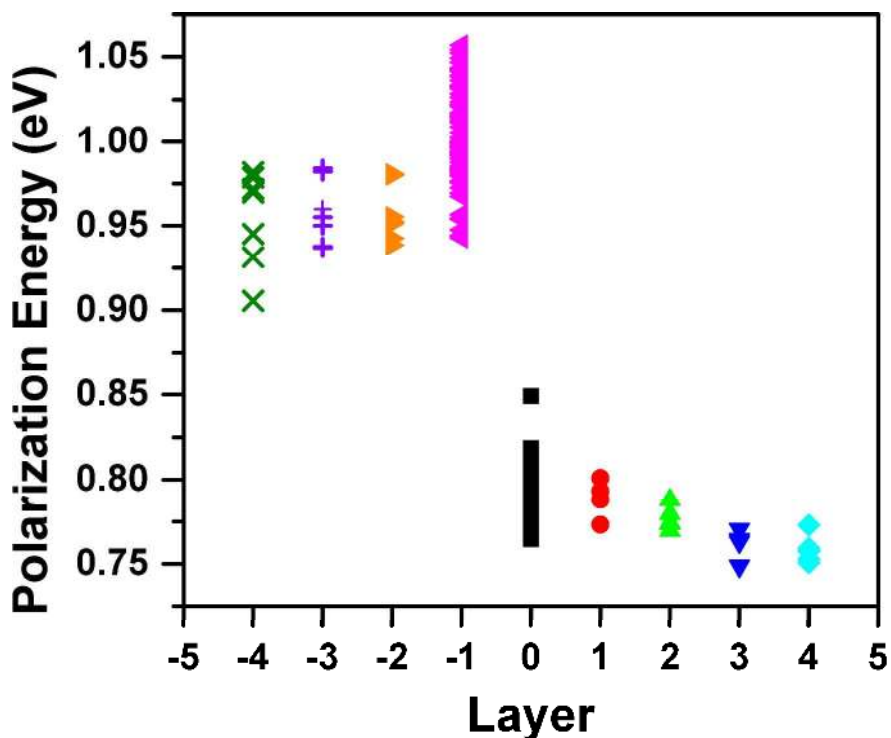


**Figure 8.** Polarization energy due to a positive charge in pentacene and negative charge in  $C_{60}$  as a function of molecular layer with respect to the interface. The  $C_{60}$  layers considered are: the  $C_{60}$  interfacial layer (■, black), 1 layer from the interface (●, red), 2 layers from the interface (▲, green), 3 layers from the interface (▼, blue), and 4 layers from the interface (◆, cyan), with the latter approximating the bulk. The pentacene layers considered are: the interfacial pentacene layer (◀, magenta), 1 layer from the interface (▶, orange), 2 layers from the interface (+, purple), and 3 layers from the interface (×, green), with the latter approximating the bulk.

A similar trend is seen on the  $C_{60}$  side of the interface. However, the polarization does not stabilize until the charge moves three layers away from the interface because the hexagonal closed packed configuration results in layers that are less well separated than in pentacene. Since the positive quadrupole component of the pentacene is pointed towards the  $C_{60}$  slab, the negative charge is more stabilized at the interface than in the bulk, which increases the polarization energy due to a negative charge at the interface, as observed for the one-dimensional systems.

1  
2  
3 While examining a single snapshot gives a picture of the disorder present at the interface at  
4 single instance in time, we also follow the individual sites in time to determine how the dynamic  
5 nature of the environment of individual sites impacts the site polarization energies (Figure 9).  
6  
7  
8 We note the the dynamic and static contributions to the disorder may also be determined, as  
9  
10 Tummala *et al.* have recently done for a series of fullerenes,<sup>59</sup> although this is outside the scope  
11  
12 of the current investigation. Snapshots were taken at 0.5 ps intervals where the polarization  
13  
14 energy at five C<sub>60</sub> sites and 19 pentacene sites was followed; each collection of sites on either  
15  
16 side of the interface occupies a similar area. Compared to the single snapshot, the polarization  
17  
18 energy distributions over the whole timespan are larger (the  $P_-$  distribution is 5% larger and the  
19  
20  $P_+$  distribution is 30% larger), indicating that the environment of the pentacene sites vary much  
21  
22 more than that of the C<sub>60</sub> sites. While it is not unexpected that the polarization energy can vary  
23  
24 by a large amount from site to site since the environment of each site is distinct, the large amount  
25  
26 over which each individual site may change is an important feature. For C<sub>60</sub>, the polarization  
27  
28 energy of a given site is observed to vary by as much as 9% (0.07 eV) with respect to its smallest  
29  
30 polarization energy, while the polarization energy of pentacene sites can vary by up to 12% (0.12  
31  
32 eV).  
33  
34  
35  
36  
37  
38  
39  
40  
41  
42  
43  
44  
45  
46  
47  
48  
49  
50  
51  
52  
53  
54  
55  
56  
57  
58  
59  
60

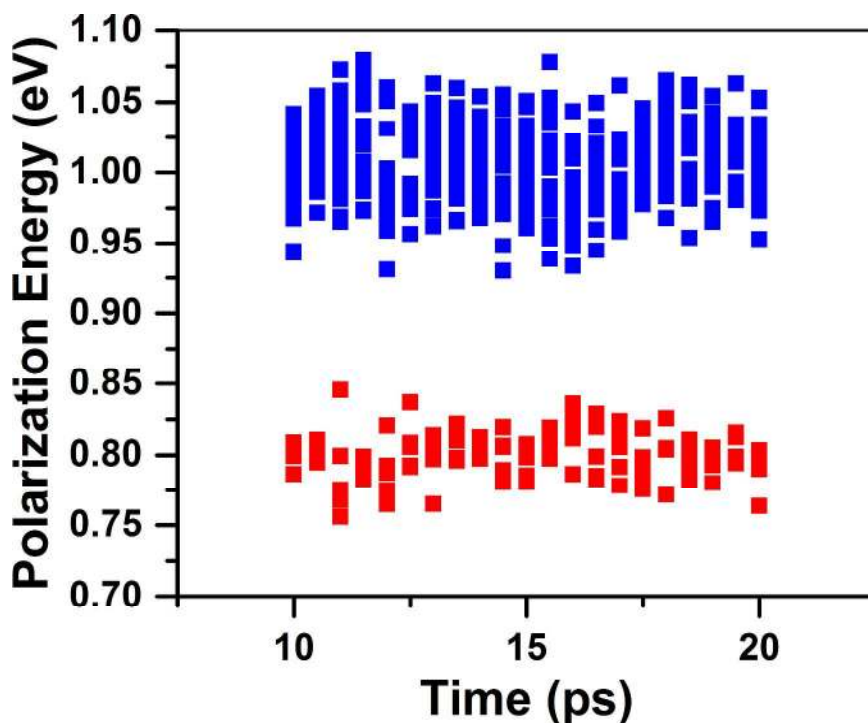


**Figure 9.** Polarization energies at selected sites of pentacene (blue) and C<sub>60</sub> (red) as a function of time in 0.5 ps increments.

### *Interface Impact on Charge Separation*

The process of exciton dissociation and charge separation is a highly debated topic in the literature.<sup>60-67</sup> The barrier, or lack thereof, to charge separation has been the focus of numerous articles with reports of barriers as large as 1.4 eV for charge separation in Alq<sub>3</sub> thin films to barriers of less than 10 meV in polymer-fullerene blends, where the charge carriers are expected to be largely delocalized.<sup>64,68-73</sup> Theoretical investigations report similar charge separation barriers and give insight into how intermolecular interactions affect this barrier:<sup>12-13</sup> (i) Yost *et al.*<sup>60</sup> showed that by modifying the bulk dielectric, molecular packing, and molecular multipole moments, the barrier to charge separation can be modified by shifting the direction and amount of band bending at the interface, which provides a driving force for charge separation; (ii) the interface geometry has been a significant focus of the work of Heremans and co-workers,<sup>12</sup> who



1  
2  
3 report the barrier to charge separation at model pentacene/C<sub>60</sub> interfaces to vary from 0.0 eV to  
4  
5 0.4 eV as a function of pentacene orientation; (iii) on the other hand, Grozema and co-workers<sup>13</sup>  
6  
7 report a barrier to charge separation in an *edge-on* pentacene/C<sub>60</sub> interface to be as large as 0.85  
8  
9 eV.  
10  
11

12  
13  
14 When a hole and electron are present at the interface, there are several interactions that occur: (i)  
15  
16 Coulombic interactions between hole and electron; (ii) charge-permanent multipole interactions  
17  
18 and charge-induced-dipole interactions between the charged molecules and their respective  
19  
20 bulks; and (iii) so-called mutual interactions due to the pentacene bulk seeing the negatively  
21  
22 charged C<sub>60</sub>, the C<sub>60</sub> bulk seeing the positively charged pentacene, as well as the static and  
23  
24 induced electrostatic interactions between the pentacene and C<sub>60</sub> slabs that are not charged.  
25  
26  
27

28  
29 To provide insight into the charge separation process and the importance of accounting for the  
30  
31 mutual interactions in addition to the Coulombic interactions, we have examined both an  
32  
33 interacting electron-hole pair and a non-interacting electron-hole pair. The energy of a  
34  
35 Coulombically-bound electron-hole pair ( $E_{EH}$ ) is defined as:  
36  
37

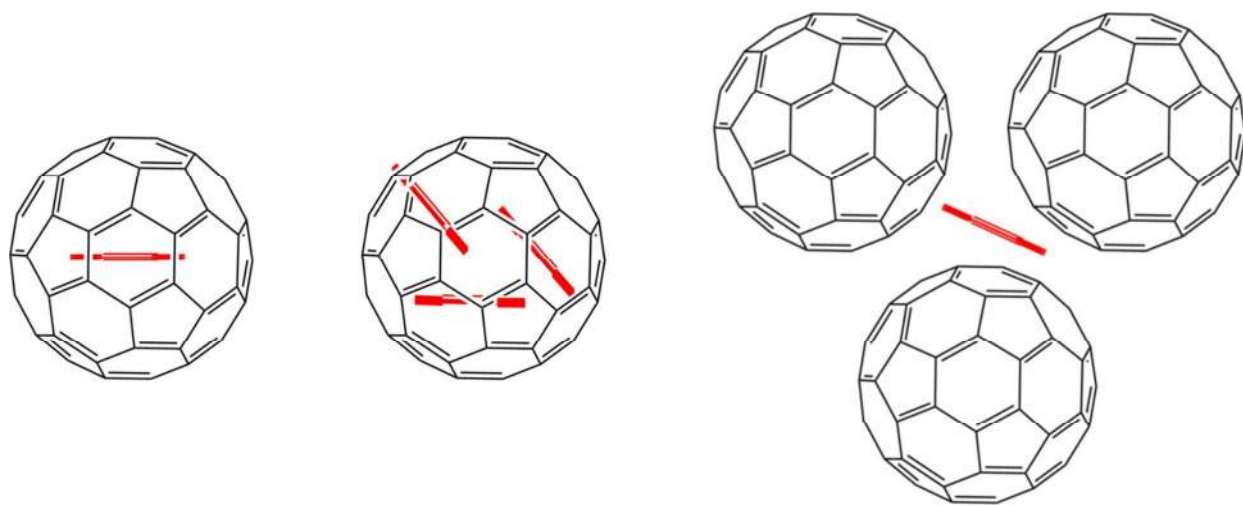
$$E_{EH} = \Delta E_{pair} - IE_{gas} - EA_{gas} \quad (6.1)$$

38  
39  
40 where  $\Delta E_{pair}$  is the change in energy of the system between the presence of the charge pair and  
41  
42 the absence of the charge pair. The energy of a non-interacting electron-hole pair ( $E_{NI-EH}$ ), that  
43  
44 is when the electron and hole do not see each other, is simply the sum of the polarization  
45  
46 energies:  
47  
48  
49  
50  
51  
52

$$E_{NI-EH} = P_+ + P_- \quad (6.2)$$

1  
2  
3  
4 where  $P_+$  and  $P_-$  may either correspond to the bulk or the interface. The comparison of  $E_{EH}$  and  
5  
6  $E_{NI-EH}$  allows the determination of the amount of mutual interaction. As we have done with the  
7  
8 polarization energy of different molecular sites, we tracked each of these quantities along a MD  
9  
10 trajectory to determine how the electrostatic environment of the electron-hole pair changes at a  
11  
12 disordered interface as a function of time.  
13  
14  
15

16  
17 Note that there are three primary configurations of pentacene and  $C_{60}$  at the pentacene/ $C_{60}$   
18  
19 interface: a first one (Figure 10, left) where  $C_{60}$  sits directly on top of a pentacene, a second one  
20  
21 (Figure 10, middle) where  $C_{60}$  sits above three neighboring pentacene (Figure 10, right), and a  
22  
23 third configuration where a pentacene sits in the space below three  $C_{60}$  molecules.  
24  
25  
26  
27  
28  
29  
30  
31  
32



52  
53 **Figure 10.** Top-down representations of the primary configurations of pentacene and  $C_{60}$  at the  
54  
55 pentacene/ $C_{60}$  interface.  
56  
57  
58  
59  
60

1  
2  
3 Looking first, for simplicity, at a single snapshot from the MD trajectory and comparing the sites  
4 within this single frame, we observe that the charge separation barrier for an electron-hole pair  
5  
6 ( $E_{CS,EH}$ ), defined as the difference in  $E_{EH}$  evaluated at the interface and in the bulk, ranges from  
7  
8 0.70 eV to 0.76 eV. These values fall between the previously reported barriers of Grozema and  
9  
10 co-workers (0.85 eV)<sup>13</sup> and Heremans and co-workers (0.44 eV).<sup>12</sup> Although the reported values  
11  
12 cover a wide range of energies, it is important to note the differences in these models; while our  
13  
14 results agree well with those of Grozema and co-workers, the microelectrostatic model  
15  
16 underestimates the charge-separation barrier. This is likely due to two factors: (i) the sub-  
17  
18 molecular representation of pentacene (described via five points) and C<sub>60</sub> (described by 12 points  
19  
20 in the microelectrostatic model), where these approximations in fact lead to an overestimation of  
21  
22 the polarizability of the molecules and cause the respective bulk regions to over-stabilize the  
23  
24 excess charges, allowing for more facile charge separation;<sup>9</sup> and (ii) the treatment of Heremans  
25  
26 and co-workers, which makes use of finite-sized spheres that are estimated to introduce  
27  
28 approximately 10% error into the charge-induced dipole interactions.  
29  
30  
31  
32  
33  
34  
35  
36  
37

38 By also evaluating the barrier for charge separation in a non-interacting electron-hole pair  
39  
40 ( $E_{CS,NI-EH}$ ), that is the difference between  $E_{NI-EH}$  evaluated at the interface and in the bulk, we  
41  
42 can determine the magnitude of the Coulomb and mutual interactions that are key to properly  
43  
44 describing the evolution from a Coulombically-bound electron-hole pair to free charge carriers in  
45  
46 the bulk. Looking at the same set of donor-acceptor sites as the interacting electron-hole pairs,  
47  
48 we determine  $E_{CS,NI-EH}$  to vary by as much as 0.13 eV from site-to-site and become as small as  
49  
50 0.02 eV. The fact that  $E_{CS,NI-EH}$  never becomes negative, although it does come within thermal  
51  
52  
53  
54  
55  
56  
57  
58  
59  
60

1  
2  
3 energy at room temperature (0.025 eV), highlights that, in the case of the pentacene(001)/C<sub>60</sub>  
4 interface, the hole and electron are more stabilized at the interface than in the bulk.  
5  
6

7  
8  
9 By comparing  $E_{CS,EH}$  and  $E_{CS,NI-EH}$ , the mutual interaction contribution, resulting from the hole,  
10 electron, and respective bulks interacting, to charge separation may be quantified. These mutual  
11 interactions account for the majority of the barrier to charge separation for the interacting pair,  
12 upwards of 90% of  $E_{CS,EH}$ . Thus, it is the change in inductive and electrostatic interactions of  
13 the environment when the two opposite charges are near each other that dictates the charge  
14 separation barrier. To minimize the barrier to charge separation, it is then necessary to reduce the  
15 contributions from these mutual interactions. One approach is the use of a *face-on* pentacene  
16 orientation; however, as stated earlier, such an orientation has been theoretically calculated to  
17 cause a large increase in the rate of charge recombination.<sup>11</sup>  
18  
19  
20  
21  
22  
23  
24  
25  
26  
27  
28  
29  
30  
31

32 This single, static picture, though, does not fully comprehend the complexity of the  
33 pentacene/C<sub>60</sub> interface, as the individual molecules move in time. For any given site, we  
34 observe that  $E_{CS,EH}$  varies by as much as 0.17 eV, nearly as much as the largest differences in  
35  $E_{CS,EH}$  observed for all sites over a range of 10 ps (0.18 eV; from 0.63 eV to 0.81 eV, Figure  
36 11). This large variation in the barrier to charge separation, while not large enough to suggest  
37 barrier-less charge separation at the pentacene/C<sub>60</sub> interface, must be considered in addition to  
38 static pictures of the charge-separation energy. Furthermore, we can separate the pentacene:C<sub>60</sub>  
39 pairs into two groups: (i) pentacenes that remain in the edge-on orientation with the neighboring  
40 fullerenes (Figure 10, left and center); and (ii) pentacenes that intercalate (at least partially) into  
41 the fullerene layer (Figure 10, right). The edge-on pentacenes have limited movement (vibration  
42  
43  
44  
45  
46  
47  
48  
49  
50  
51  
52  
53  
54  
55  
56  
57  
58  
59  
60

within the layer), as they are constrained to the pentacene layer. Thus, the change in charge separation for these sites is relatively small, about 0.09 eV.

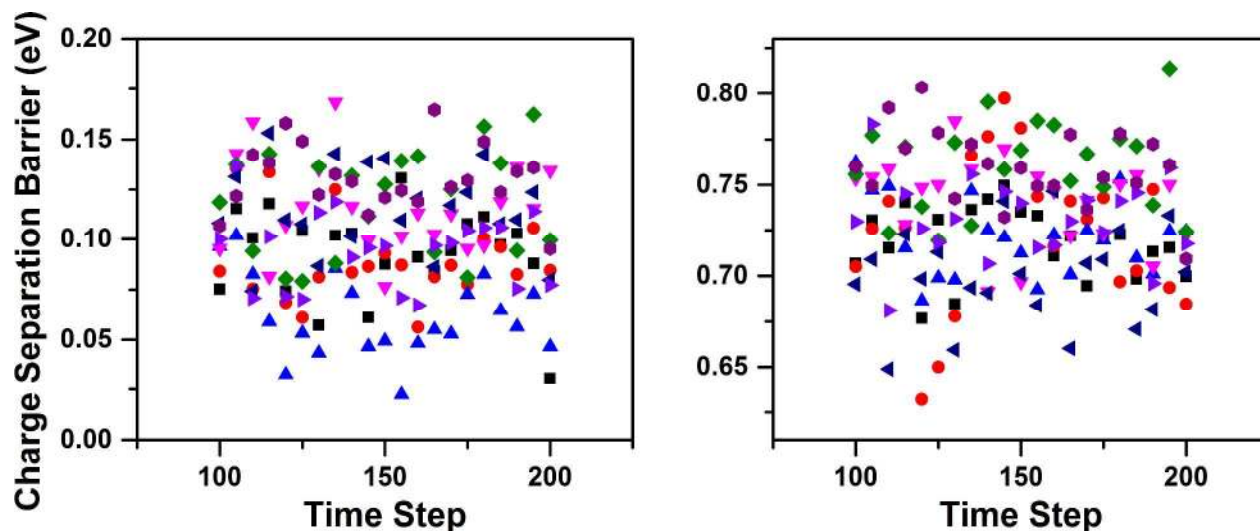


**Figure 11.** (Left) Charge separation barrier for a non-interacting electron-hole pair for eight pairs. (Right) Charge separation barrier for an interacting electron-hole pair for eight pairs. Symbols correspond to individual pentacene/ $C_{60}$  pairs as they are followed along the MD trajectory.

On the other hand, those pentacenes that are able to move partially into the fullerene layer experience a significant change in charge separation barrier. Over a period of about 7 ps, the pentacene can slide away from the pentacene interface, where the charge separation barrier is at a minimum due to the large distance between the hole and electron, to a position where approximately one fused ring is out of the pentacene layer, protruding into the  $C_{60}$  layer. At this latter position, the charge-separation barrier becomes large due to the closer proximity of the

1  
2  
3 hole and electron. The pentacene can then translate back down to the pentacene layer. Along this  
4  
5 course of motion, the charge-separation barrier can change by almost 0.2 eV (Figure S4).  
6  
7

8  
9 This motion provides a more complex picture of charge separation in these systems by opening  
10  
11 additional pathways for consideration. From a positively minded perspective, one could envision  
12  
13 a scenario where a charge transfer state is formed when the pentacene is in a partially  
14  
15 intercalated state, leading to a maximized electronic coupling; then as the pentacene moves back  
16  
17 into the pentacene domain, the hole can partially delocalize within this layer and the barrier to  
18  
19 charge separation is reduced allowing for more easy separation of the hole and electron into free  
20  
21 charge carriers.  
22  
23  
24  
25  
26  
27  
28  
29

### 30 **Synopsis**

31  
32  
33 Through a combination of quantum-mechanics calculations and molecular-mechanics and  
34  
35 molecular-dynamics simulations, we have investigated the effect of the bulk organic material and  
36  
37 of an organic-organic interface on the energy of an excess charge carrier. By using molecular  
38  
39 dynamics simulations, we have shown that a simple static picture of the interface between two  
40  
41 organic slabs is not sufficient to properly describe the dynamic nature of these complex  
42  
43 interfaces present in the active layers of OPV devices. In the bulk materials, we calculate that a  
44  
45 positive charge in pentacene is more stabilized by its environment than a negative charge in C<sub>60</sub>  
46  
47 (by about 0.27 eV), in agreement with available experimental estimates; for both pentacene and  
48  
49 C<sub>60</sub>, an excess charge is more stabilized, *i.e.*, has a larger polarization energy, at the interface  
50  
51 than in the bulk, in contrast to the behavior observed at an organic-vacuum interface.<sup>29</sup>  
52  
53  
54  
55  
56  
57  
58  
59  
60

1  
2  
3 Moving beyond simply gluing two organic slabs together, we examined a bulk *edge-on*  
4  
5 pentacene/C<sub>60</sub> interface after 1 ns of molecular dynamics simulation at room temperature to  
6  
7 determine how the energetic landscape changes in time. From the results of these MD  
8  
9 simulations, we obtain that:  
10  
11

- 12  
13  
14 • Each site along the interface feels a unique electrostatic environment that determines its  
15  
16 polarization energy and results from the instantaneous positions of all neighboring  
17  
18 molecules.  
19
- 20  
21 • There exists a distribution of polarization energies at the interface, in contrast to the  
22  
23 bulk where each site is essentially equivalent.  
24
- 25  
26 • In general, an excess charge at the pentacene/C<sub>60</sub> interface is more stabilized than in the  
27  
28 bulk; however, since the electrostatic environment of each site can change significantly  
29  
30 in time, this does not always hold true.  
31
- 32  
33 • The barrier to charge separation for an electron-hole pair at the pentacene(001)/C<sub>60</sub>  
34  
35 interface is about 0.75 eV, but can vary by as much as 25% for a given site in time.  
36

37  
38 Thus, a major conclusion that can be drawn is that the *dynamic* nature of the interface results in  
39  
40 large changes in the energetic landscape on a short timescale, which must be accounted for in  
41  
42 discussions of charge separation in OPV devices.  
43  
44

45  
46 Our work underlines that the energetic landscape at a bilayer interface is more complex than is  
47  
48 often considered, with the environment of each molecular site changing considerably over time.

49  
50 While the charge separation energies that we have reported here would seem to indicate that  
51  
52 efficient charge separation is not possible in such bilayer configurations, we note that there are  
53  
54 several effects that would act to reduce or negate this large barrier:  
55  
56  
57  
58  
59  
60

- 1  
2  
3 (i) As has been recently shown,<sup>74</sup> the static multipole moments at the interface can be  
4 tuned to promote efficient charge separation and lead to high-performance OPV  
5 devices.  
6  
7  
8  
9  
10 (ii) By increasing the dimensionality of the charge transport in the active materials of  
11 OPVs, the entropy of the system can increase and result in more efficient charge  
12 separation.<sup>75</sup>  
13  
14  
15 (iii) Charge delocalization would increase the mean distance between charge centers;<sup>76-77</sup>  
16 thus, delocalization combined with the changing barrier to charge separation due to  
17 motions in and out-of the molecular plane, can act to decrease the magnitude of the  
18 charge-separation barrier.  
19  
20  
21  
22  
23  
24  
25  
26

27 Indeed, there are a number of interactions and phenomena that must be considered and  
28 accounted for in an integrated model if we are to understand in detail the processes that occur  
29 at organic-organic interfaces.  
30  
31  
32  
33  
34  
35  
36  
37  
38  
39  
40  
41  
42  
43  
44  
45  
46  
47  
48  
49  
50  
51  
52  
53  
54  
55  
56  
57  
58  
59  
60



1  
2  
3  
4  
5  
6  
7  
8  
9  
10 **Acknowledgements.** This work has been supported by King Abdullah University of Science and  
11 Technology (KAUST), the KAUST Competitive Research Grant program, and the Office of  
12 Naval Research Global (Award N62909-15-1-2003). We acknowledge the IT Research  
13 Computing Team and Supercomputing Laboratory at KAUST for providing computational and  
14 storage resources. This work has also used the computing resources of the Garnet, Spirit, and  
15 Copper supercomputing systems through the DoD HPCMP. C.R. thanks the University of  
16 Kentucky Vice President of Research for start-up funds. We wish to thank Mahesh Kumar Ravva  
17 and Naga Rajesh Tummala for stimulating discussions and assistance with technical elements of  
18 the molecular dynamics simulations.  
19  
20  
21  
22  
23  
24  
25  
26  
27  
28  
29  
30  
31  
32  
33  
34  
35

36 **Supporting Information Available:** A qualitative description of the difference in overall  
37 system order in the minimized and MD interfaces, the single-molecule structures used for the  
38 parameterization of the AMOEBA force field, and the crystal structure of C<sub>60</sub> generated via the  
39 Materials Studio suite, are available in the Supporting Information. This material is available free  
40 of charge via the Internet at <http://pubs.acs.org>.  
41  
42  
43  
44  
45  
46  
47  
48  
49  
50  
51  
52  
53  
54  
55  
56  
57  
58  
59  
60

## References

1. NREL NREL Best Research-Cell Efficiencies.  
[http://www.nrel.gov/ncpv/images/efficiency\\_chart.jpg](http://www.nrel.gov/ncpv/images/efficiency_chart.jpg) (accessed April 13).
2. Heliatek Heliatek Sets New Organic Photovoltaic World Record Efficiency of 13.2%.  
<http://www.heliatek.com/en/press/press-releases/details/heliatek-sets-new-organic-photovoltaic-world-record-efficiency-of-13-2> (accessed March 7).
3. Zhao, J.; Li, Y.; Yang, G.; Jiang, K.; Lin, H.; Ade, H.; Ma, W.; Yan, H., Efficient Organic Solar Cells Processed from Hydrocarbon Solvents. *Nat. Energy* **2016**, *1*, 15027.
4. Liu, Y.; Zhao, J.; Li, Z.; Mu, C.; Ma, W.; Hu, H.; Jiang, K.; Lin, H.; Ade, H.; Yan, H., Aggregation and Morphology Control Enables Multiple Cases of High-Efficiency Polymer Solar Cells. *Nat. Commun* **2014**, *5*, 5293.
5. Hu, H.; Jiang, K.; Yang, G.; Liu, J.; Li, Z.; Lin, H.; Liu, Y.; Zhao, J.; Zhang, J.; Huang, F.; Qu, Y.; Ma, W.; Yan, H., Terthiophene-Based D–A Polymer with an Asymmetric Arrangement of Alkyl Chains That Enables Efficient Polymer Solar Cells. *J. Am. Chem. Soc.* **2015**, *137*, 14149-14157.
6. Bredas, J. L.; Norton, J. E.; Cornil, J.; Coropceanu, V., Molecular Understanding of Organic Solar Cells: The Challenges. *Acc. Chem. Res.* **2009**, *42*, 1691-1699.
7. Lyons, B. P.; Clarke, N.; Groves, C., The Relative Importance of Domain Size, Domain Purity and Domain Interfaces to the Performance of Bulk-Heterojunction Organic Photovoltaics. *Ener. Envir. Sci.* **2012**, *5*, 7657-7663.
8. Yan, H.; Swaraj, S.; Wang, C.; Hwang, I.; Greenham, N. C.; Groves, C.; Ade, H.; McNeill, C. R., Influence of Annealing and Interfacial Roughness on the Performance of Bilayer Donor/Acceptor Polymer Photovoltaic Devices. *Adv. Funct. Mater.* **2010**, *20*, 4329-4337.
9. Linares, M.; Beljonne, D.; Cornil, J. r. m.; Lancaster, K.; Brédas, J.-L.; Verlaak, S.; Mityashin, A.; Heremans, P.; Fuchs, A.; Lennartz, C.; Idé, J.; Méreau, R. I.; Aurel, P.; Ducasse, L.; Castet, F. d. r., On the Interface Dipole at the Pentacene–Fullerene Heterojunction: A Theoretical Study. *J. Phys. Chem. C* **2010**, *114*, 3215-3224.
10. Mothy, S.; Guillaume, M.; Idé, J.; Castet, F.; Ducasse, L.; Cornil, J.; Beljonne, D., Tuning the Interfacial Electronic Structure at Organic Heterojunctions by Chemical Design. *J. Phys. Chem. Lett.* **2012**, *3*, 2374-2378.
11. Yi, Y. P.; Coropceanu, V.; Bredas, J. L., Exciton-Dissociation and Charge-Recombination Processes in Pentacene/C60Solar Cells. *J. Am. Chem. Soc.* **2009**, *131*, 15777-15783.
12. Verlaak, S.; Beljonne, D.; Cheyins, D.; Rolin, C.; Linares, M.; Castet, F.; Cornil, J.; Heremans, P., Electronic Structure and Geminate Pair Energetics at Organic–Organic Interfaces: The Case of Pentacene/C60 Heterojunctions. *Adv. Funct. Mater.* **2009**, *19*, 3809-3814.
13. Gorczak, N.; Swart, M.; Grozema, F. C., Energetics of Charges in Organic Semiconductors and at Organic Donor-Acceptor Interfaces. *J. Mater. Chem. C* **2014**, *2*, 3467-3475.
14. Castet, F.; D'Avino, G.; Muccioli, L.; Cornil, J.; Beljonne, D., Charge Separation Energetics at Organic Heterojunctions: On the Role of Structural and Electrostatic Disorder. *Phys. Chem. Chem. Phys.* **2014**, *16*, 20279-20290.
15. Beljonne, D.; Cornil, J.; Muccioli, L.; Zannoni, C.; Bredas, J. L.; Castet, F., Electronic Processes at Organic–Organic Interfaces: Insight from Modeling and Implications for Optoelectronic Devices. *Chem. Mater.* **2011**, *23*, 591-609.

16. Chen, W.; Nikiforov, M. P.; Darling, S. B., Morphology Characterization in Organic and Hybrid Solar Cells. *Ener. Envir. Sci.* **2012**, *5*, 8045-8074.
17. Liao, H.-C.; Ho, C.-C.; Chang, C.-Y.; Jao, M.-H.; Darling, S. B.; Su, W.-F., Additives for Morphology Control in High-Efficiency Organic Solar Cells. *Mater. Today* **2013**, *16*, 326-336.
18. Coakley, K. M.; McGehee, M. D., Conjugated Polymer Photovoltaic Cells. *Chem. Mater.* **2004**, *16*, 4533-4542.
19. Casalegno, M.; Carbonera, C.; Luzzati, S.; Raos, G., Coarse-Grained Kinetic Modelling of Bilayer Heterojunction Organic Solar Cells. *Org. Elect.* **2012**, *13*, 750-761.
20. Bartelt, J. A.; Beiley, Z. M.; Hoke, E. T.; Mateker, W. R.; Douglas, J. D.; Collins, B. A.; Tumbleston, J. R.; Graham, K. R.; Amassian, A.; Ade, H.; Fréchet, J. M. J.; Toney, M. F.; McGehee, M. D., The Importance of Fullerene Percolation in the Mixed Regions of Polymer–Fullerene Bulk Heterojunction Solar Cells. *Adv. Energy Mater.* **2013**, *3*, 364-374.
21. Fu, Y.-T.; Risko, C.; Brédas, J.-L., Intermixing at the Pentacene-Fullerene Bilayer Interface: A Molecular Dynamics Study. *Adv. Mater.* **2013**, *25*, 878-882.
22. Correia, H. M. G.; Barbosa, H. M. C.; Marques, L.; Ramos, M. M. D., Understand the Importance of Molecular Organization at Polymer–Polymer Interfaces in Excitonic Solar Cells. *Thin Solid Films* **2014**, *560*, 59-64.
23. Bloking, J. T.; Giovenzana, T.; Higgs, A. T.; Ponec, A. J.; Hoke, E. T.; Vandewal, K.; Ko, S.; Bao, Z.; Sellinger, A.; McGehee, M. D., Comparing the Device Physics and Morphology of Polymer Solar Cells Employing Fullerenes and Non-Fullerene Acceptors. *Adv. Energy Mater.* **2014**, *4*, 1301426.
24. Mladenović, M.; Vukmirović, N., Charge Carrier Localization and Transport in Organic Semiconductors: Insights from Atomistic Multiscale Simulations. *Adv. Funct. Mater.* **2015**, *25*, 1915-1932.
25. Gehrig, D. W.; Howard, I. A.; Sweetnam, S.; Burke, T. M.; McGehee, M. D.; Laquai, F., The Impact of Donor–Acceptor Phase Separation on the Charge Carrier Dynamics in pBTTT:PCBM Photovoltaic Blends. *Macromol. Rapid Commun.* **2015**, *36*, 1054-1060.
26. Buchaca-Domingo, E.; Vandewal, K.; Fei, Z.; Watkins, S. E.; Scholes, F. H.; Bannock, J. H.; de Mello, J. C.; Richter, L. J.; DeLongchamp, D. M.; Amassian, A.; Heeney, M.; Salleo, A.; Stingelin, N., Direct Correlation of Charge Transfer Absorption with Molecular Donor:Acceptor Interfacial Area via Photothermal Deflection Spectroscopy. *J. Am. Chem. Soc.* **2015**, *137*, 5256-5259.
27. Noriega, R.; Rivnay, J.; Vandewal, K.; Koch, F. P. V.; Stingelin, N.; Smith, P.; Toney, M. F.; Salleo, A., A General Relationship Between Disorder, Aggregation and Charge Transport in Conjugated Polymers. *Nat. Mater.* **2013**, *12*, 1038-1044.
28. Collins, B. A.; Tumbleston, J. R.; Ade, H., Miscibility, Crystallinity, and Phase Development in P3HT/PCBM Solar Cells: Toward an Enlightened Understanding of Device Morphology and Stability. *J. Phys. Chem. Lett.* **2011**, *2*, 3135-3145.
29. Ryno, S. M.; Risko, C.; Bredas, J. L., Impact of Molecular Orientation and Packing Density on Electronic Polarization in the Bulk and at Surfaces of Organic Semiconductors. *ACS Appl. Mater. Interfaces* **2016**, DOI: 10.1021/acsami.6b02579.
30. Ryno, S. M.; Lee, S. R.; Sears, J.; Risko, C.; Bredas, J. L., Electronic Polarization Effects upon Charge Injection in Oligoacene Molecular Crystals: Description via a Polarizable Force Field. *J. Phys. Chem. C* **2013**, *117*, 13853-13860.

- 1  
2  
3  
4  
5  
6  
7  
8  
9  
10  
11  
12  
13  
14  
15  
16  
17  
18  
19  
20  
21  
22  
23  
24  
25  
26  
27  
28  
29  
30  
31  
32  
33  
34  
35  
36  
37  
38  
39  
40  
41  
42  
43  
44  
45  
46  
47  
48  
49  
50  
51  
52  
53  
54  
55  
56  
57  
58  
59  
60
31. Ryno, S. M.; Risko, C.; Brédas, J.-L., Impact of Molecular Packing on Electronic Polarization in Organic Crystals: The Case of Pentacene vs TIPS-Pentacene. *J. Am. Chem. Soc.* **2014**, *136*, 6421-6427.
32. Ren, P.; Ponder, J. W., Consistent Treatment of Inter- and Intramolecular Polarization in Molecular Mechanics Calculations. *J. Comput. Chem.* **2002**, *23*, 1497-1506.
33. Ponder, J. W.; Wu, C.; Ren, P.; Pande, V. S.; Chodera, J. D.; Schnieders, M. J.; Haque, I.; Mobley, D. L.; Lambrecht, D. S.; DiStasio, R. A.; Head-Gordon, M.; Clark, G. N. I.; Johnson, M. E.; Head-Gordon, T., Current Status of the AMOEBA Polarizable Force Field. *J. Phys. Chem. B* **2010**, *114*, 2549-2564.
34. Allen, F. H., The Cambridge Structural Database: A Quarter Million Crystal Structures and Rising. *Acta Crystallogr.* **2002**, *B58*, 380-388.
35. Mattheus, C. C.; Dros, A. B.; Baas, J.; Meetsma, A.; Boer, J. L. d.; Palstra, T. T. M., Polymorphism in Pentacene. *Acta Crystallogr., Sect. C: Cryst. Struct. Commun.* **2001**, *57*, 939.
36. Bürgi, H.-B.; Blanc, E.; Schwarzenbach, D.; Liu, S.; Lu, Y.-j.; Kappes, M. M.; Ibers, J. A., The Structure of C60: Orientational Disorder in the Low-Temperature Modification of C60. *Angew. Chem., Int. Ed. Engl.* **1992**, *31*, 640-643.
37. Stone, A. J., Distributed Multipole Analysis: Stability for Large Basis Sets. *J. Chem. Theory Comput.* **2005**, *1*, 1128-1132.
38. Frisch, M. J.; Trucks, G. W.; Schlegel, H. B.; Scuseria, G. E.; Robb, M. A.; Cheeseman, J. R.; Scalmani, G.; Barone, V.; Mennucci, B.; Petersson, G. A.; Nakatsuji, H.; Caricato, M.; Li, X.; Hratchian, H. P.; Izmaylov, A. F.; Bloino, J.; Zheng, G.; Sonnenberg, J. L.; Hada, M.; Ehara, M.; Toyota, K.; Fukuda, R.; Hasegawa, J.; Ishida, M.; Nakajima, T.; Honda, Y.; Kitao, O.; Nakai, H.; Vreven, T.; Montgomery Jr., J. A.; Peralta, J. E.; Ogliaro, F.; Bearpark, M. J.; Heyd, J.; Brothers, E. N.; Kudin, K. N.; Staroverov, V. N.; Kobayashi, R.; Normand, J.; Raghavachari, K.; Rendell, A. P.; Burant, J. C.; Iyengar, S. S.; Tomasi, J.; Cossi, M.; Rega, N.; Millam, N. J.; Klene, M.; Knox, J. E.; Cross, J. B.; Bakken, V.; Adamo, C.; Jaramillo, J.; Gomperts, R.; Stratmann, R. E.; Yazyev, O.; Austin, A. J.; Cammi, R.; Pomelli, C.; Ochterski, J. W.; Martin, R. L.; Morokuma, K.; Zakrzewski, V. G.; Voth, G. A.; Salvador, P.; Dannenberg, J. J.; Dapprich, S.; Daniels, A. D.; Farkas, Ö.; Foresman, J. B.; Ortiz, J. V.; Cioslowski, J.; Fox, D. J. *Gaussian 09*, Gaussian, Inc.: Wallingford, CT, USA, 2009.
39. Gastel, M. v., Zero-Field Splitting of the Lowest Excited Triplet States of C60 and C70 and Benzene. *J. Phys. Chem. A* **2010**, *114*, 10864-10870.
40. Green, W. H.; Gorun, S. M.; Fitzgerald, G.; Fowler, P. W.; Ceulemans, A.; Titeca, B. C., Electronic Structures and Geometries of C60 Anions via Density Functional Calculations. *J. Phys. Chem.* **1996**, *100*, 14892-14898.
41. Note that previous electronic-structure calculations have shown the calculated charge distribution of fullerene anion to be highly sensitive to the amount of included Hartree-Fock exchange.
42. Lyons, L., Ionized States of Molecular Crystals. *Aust. J. Chem.* **1957**, *10*, 365-367.
43. Silinsh, E. A., *Organic Molecular Crystals: Their Electronic States*. Springer: New York, 1980.
44. Lii, J. H.; Allinger, N. L., Molecular Mechanics. The MM3 Force Field for Hydrocarbons. 3. The van der Waals' Potentials and Crystal Data for Aliphatic and Aromatic Hydrocarbons. *J. Am. Chem. Soc.* **1989**, *111*, 8576-8582.

- 1  
2  
3  
4  
5  
6  
7  
8  
9  
10  
11  
12  
13  
14  
15  
16  
17  
18  
19  
20  
21  
22  
23  
24  
25  
26  
27  
28  
29  
30  
31  
32  
33  
34  
35  
36  
37  
38  
39  
40  
41  
42  
43  
44  
45  
46  
47  
48  
49  
50  
51  
52  
53  
54  
55  
56  
57  
58  
59  
60
45. Swope, W. C.; Andersen, H. C.; Berens, P. H.; Wilson, K. R., A Computer Simulation Method for the Calculation of Equilibrium Constants for the Formation of Physical Clusters of Molecules: Application to Small Water Clusters. *J. Chem. Phys.* **1982**, *76*, 637-649.
46. Berendsen, H. J. C.; Postma, J. P. M.; van Gunsteren, W. F.; DiNola, A.; Haak, J. R., Molecular Dynamics with Coupling to an External Bath. *J. Chem. Phys.* **1984**, *81*, 3684-3690.
47. Darden, T.; York, D.; Pedersen, L., Particle Mesh Ewald: An  $N \cdot \log(N)$  Method for Ewald Sums in Large Systems. *J. Chem. Phys.* **1993**, *98*, 10089-10092.
48. Andersen, H. C., Rattle: A “Velocity” Version of the Shake Algorithm for Molecular Dynamics Calculations. *J. Comput. Phys.* **1983**, *52*, 24-34.
49. Ponder, J. W. *TINKER: Software Tools for Molecular Design*, 2015.
50. Sato, N.; Seki, K.; Inokuchi, H., Polarization Energies of Organic Solids Determined by Ultraviolet Photoelectron Spectroscopy. *J. Chem. Soc., Faraday Trans. 2* **1981**, *77*, 1621-1633.
51. Sato, N.; Inokuchi, H.; Silinsh, E. A., Reevaluation of Electronic Polarization Energies in Organic Molecular Crystals. *Chem. Phys.* **1987**, *115*, 269-277.
52. Qi, Y.; Mohapatra, S. K.; Kim, S. B.; Barlow, S.; Marder, S. R.; Kahn, A., Solution Doping of Organic Semiconductors Using Air-Stable n-Dopants. *Appl. Phys. Lett.* **2012**, *100*, 083305.
53. Chan, C.; Kahn, A., N-Doping of Pentacene by Decamethylcobaltocene. *Appl. Phys. A* **2009**, *95*, 7-13.
54. Sato, N.; Saito, Y.; Shinohara, H., Threshold Ionization Energy of C60 in the Solid State. *Chem. Phys.* **1992**, *162*, 433-438.
55. Yoshida, H., Low-Energy Inverse Photoemission Study on the Electron Affinities of Fullerene Derivatives for Organic Photovoltaic Cells. *J. Phys. Chem. C* **2014**, *118*, 24377-24382.
56. Lichtenberger, D. L.; Nebesny, K. W.; Ray, C. D.; Huffman, D. R.; Lamb, L. D., Valence and Core Photoelectron Spectroscopy of C60, Buckminsterfullerene. *Chem. Phys. Lett.* **1991**, *176*, 203-208.
57. Idé, J.; Mothy, S.; Savoyant, A.; Fritsch, A.; Aurel, P.; Méreau, R.; Ducasse, L.; Cornil, J.; Beljonne, D.; Castet, F., Interfacial Dipole and Band Bending in Model Pentacene/C60 Heterojunctions. *Int. J. Quantum Chem.* **2013**, *113*, 580-584.
58. We note that there is an approximately 10% error associated with using the polarization energy of a finite-sized sphere instead of the extrapolated values, as is typically done for the bulk, in this analysis.
59. Tummala, N. R.; Zheng, Z.; Aziz, S. G.; Coropceanu, V.; Brédas, J.-L., Static and Dynamic Energetic Disorders in the C60, PC61BM, C70, and PC71BM Fullerenes. *J. Phys. Chem. Lett.* **2015**, *6*, 3657-3662.
60. Yost, S. R.; Van Voorhis, T., Electrostatic Effects at Organic Semiconductor Interfaces: A Mechanism for “Cold” Exciton Breakup. *J. Phys. Chem. C* **2013**, *117*, 5617-5625.
61. Heeger, A. J., 25th Anniversary Article: Bulk Heterojunction Solar Cells: Understanding the Mechanism of Operation. *Adv. Mater.* **2014**, *26*, 10-28.
62. Tvingstedt, K.; Vandewal, K.; Zhang, F.; Inganäs, O., On the Dissociation Efficiency of Charge Transfer Excitons and Frenkel Excitons in Organic Solar Cells: A Luminescence Quenching Study. *J. Phys. Chem. C* **2010**, *114*, 21824-21832.
63. Jailaubekov, A. E.; Willard, A. P.; Tritsch, J. R.; Chan, W.-L.; Sai, N.; Gearba, R.; Kaake, L. G.; Williams, K. J.; Leung, K.; Rossky, P. J.; Zhu, X. Y., Hot Charge-Transfer Excitons Set the Time Limit for Charge Separation at Donor/Acceptor Interfaces in Organic Photovoltaics. *Nat. Mater.* **2013**, *12*, 66-73.

- 1  
2  
3  
4  
5  
6  
7  
8  
9  
10  
11  
12  
13  
14  
15  
16  
17  
18  
19  
20  
21  
22  
23  
24  
25  
26  
27  
28  
29  
30  
31  
32  
33  
34  
35  
36  
37  
38  
39  
40  
41  
42  
43  
44  
45  
46  
47  
48  
49  
50  
51  
52  
53  
54  
55  
56  
57  
58  
59  
60
64. Clarke, T. M.; Durrant, J. R., Charge Photogeneration in Organic Solar Cells. *Chem. Rev.* **2010**, *110*, 6736-6767.
65. Deibel, C.; Strobel, T.; Dyakonov, V., Role of the Charge Transfer State in Organic Donor–Acceptor Solar Cells. *Adv. Mater.* **2010**, *22*, 4097-4111.
66. Etzold, F.; Howard, I. A.; Mauer, R.; Meister, M.; Kim, T.-D.; Lee, K.-S.; Baek, N. S.; Laquai, F., Ultrafast Exciton Dissociation Followed by Nongeminate Charge Recombination in PCDTBT:PCBM Photovoltaic Blends. *J. Am. Chem. Soc.* **2011**, *133*, 9469-9479.
67. Vandewal, K.; Albrecht, S.; Hoke, E. T.; Graham, K. R.; Widmer, J.; Douglas, J. D.; Schubert, M.; Mateker, W. R.; Bloking, J. T.; Burkhard, G. F.; Sellinger, A.; Fréchet, J. M. J.; Amassian, A.; Riede, M. K.; McGehee, M. D.; Neher, D.; Salero, A., Efficient Charge Generation by Relaxed Charge-Transfer States at Organic Interfaces. *Nat. Mater.* **2014**, *13*, 63-68.
68. Hill, I. G.; Kahn, A.; Soos, Z. G.; Pascal, J. R. A., Charge-Separation Energy in Films of  $\pi$ -Conjugated Organic Molecules. *Chem. Phys. Lett.* **2000**, *327*, 181-188.
69. Pensack, R. D.; Asbury, J. B., Barrierless Free Carrier Formation in an Organic Photovoltaic Material Measured with Ultrafast Vibrational Spectroscopy. *J. Am. Chem. Soc.* **2009**, *131*, 15986-15987.
70. Deibel, C.; Strobel, T.; Dyakonov, V., Origin of the Efficient Polaron-Pair Dissociation in Polymer-Fullerene Blends. *Phys. Rev. Lett.* **2009**, *103*, 036402.
71. Durrant, J. R., Molecular Approaches to Solar Energy Conversion: The Energetic Cost of Charge Separation from Molecular-Excited States. *Phil. Trans. R. Soc. A* **2013**, *371*, 20120195.
72. Murthy, D. H. K.; Gao, M.; Vermeulen, M. J. W.; Siebbeles, L. D. A.; Savenije, T. J., Mechanism of Mobile Charge Carrier Generation in Blends of Conjugated Polymers and Fullerenes: Significance of Charge Delocalization and Excess Free Energy. *J. Phys. Chem. C* **2012**, *116*, 9214-9220.
73. Jeong, K. S.; Pensack, R. D.; Asbury, J. B., Vibrational Spectroscopy of Electronic Processes in Emerging Photovoltaic Materials. *Acc. Chem. Res.* **2013**, *46*, 1538-1547.
74. Poelking, C.; Tietze, M.; Elschner, C.; Olthof, S.; Hertel, D.; Baumeier, B.; Würthner, F.; Meerholz, K.; Leo, K.; Andrienko, D., Impact of Mesoscale Order on Open-Circuit Voltage in Organic Solar Cells. *Nat. Mater.* **2015**, *14*, 434-439.
75. Gregg, B. A., Entropy of Charge Separation in Organic Photovoltaic Cells: The Benefit of Higher Dimensionality. *J. Phys. Chem. Lett.* **2011**, *2*, 3013-3015.
76. Yoshida, H.; Yamada, K.; Tsutsumi, J. y.; Sato, N., Complete Description of Ionization Energy and Electron Affinity in Organic Solids: Determining Contributions from Electronic Polarization, Energy Band Dispersion, and Molecular Orientation. *Phys. Rev. B* **2015**, *92*, 075145.
77. Bakulin, A. A.; Rao, A.; Pavelyev, V. G.; van Loosdrecht, P. H. M.; Pshenichnikov, M. S.; Niedzialek, D.; Cornil, J.; Beljonne, D.; Friend, R. H., The Role of Driving Energy and Delocalized States for Charge Separation in Organic Semiconductors. *Science* **2012**, *335*, 1340-1344.

## Table of Contents Figure

